High Performance Three-Dimensional Chemical Sensor Platform Using Reduced Graphene Oxide Formed on High Aspect-Ratio Micro-Pillars

*Le Thai Duy, Duck-Jin Kim, Tran Quang Trung, Vinh Quang Dang, Bo-Yeong Kim, Hock Key Moon, and Nae-Eung Lee**

The sensing performance of chemical sensors can be achieved not only by modification or hybridization of sensing materials but also through new design in device geometry. The performance of a chemical sensing device can be enhenced from a simple three-dimensional (3D) chemiresistor-based gas sensor platform with an increased surface area by forming networked, self-assembled reduced graphene oxide (R-GO) nanosheets on 3D SU8 micro-pillar arrays. The 3D R-GO sensor is highly responsive to low concentration of ammonia (NH_3) and nitrogen dioxide (NO_2) diluted in dry air at room temperature. Compared to the two-dimensional planar R-GO sensor structure, as the result of the increase in sensing area and interaction cross-section of R-GO on the same device area, the 3D R-GO gas sensors show improved sensing performance with faster response (about 2%/s exposure), higher sensitivity, and even a possibly lower limit of detection towards NH_3 at room temperature.

1. Introduction

Nowadays, with the rapid increase of extreme demands on our work life, not only industry but also agriculture has sustained a considerable increase in the demands of work load. To boost productivity and performance, an increasing number of toxic, flammable, and combustible chemicals and gases have been produced and consumed. However, emission of harmful by-products and pollutants, such as nitrogen oxides (NO_x), carbon oxides (CO_x), sulfur oxides (SO_x), ammonia (NH_3) and so on, have also increased significantly and endangered our health and environment over the long term. To monitor chemical materials harmful to human health and the environment, chemical sensing devices have been extensively developed and used. Improvement and optimization of present chemical sensors, including gas sensors as well as the development of new sensors that possess higher sensing performance with higher sensitivity but lower cost, are still necessary for not only industrial but also indoor health and safety, environmental monitoring, and beyond.[1–3]

Recently, extensive researches have been performed on gas sensors based on low-dimensional materials of nanowires, nanodots, and nanosheets due to their advantages such as high sensitivity, low limit of detection (LOD), and sensing capability in favorable conditions.[2–7] Within those sensing materials, graphene (Gr) has also attracted considerable attention and shown significant potential for future applications.[6,8] The main reason for this potential is Gr's unique surface-to-volume ratio. Gr has an abundant surface area for reactions to occur, resulting in the domination of surface effects. The increase of the surface area of Gr therefore could lead to the enhancement of related properties such as catalytic activity or surface adsorption and reaction, which are cardinal factors for superior-gas-sensor production.[9] Gr also shows potential due to its excellent electrical properties at room temperature and the ultra-sensitivity of charge transport through Gr to the adsorption of various analyte molecules (which act as electron/hole donors or acceptors, leading to changes in the conductance of Gr), such as pollutants (NO_2,[10–12] CO,[10] NH_3,[10–13] etc.), harmful volatile organic compounds (methanol,[14,15] toluene,[15,16] etc.) and so on. Furthermore, the responsiveness of Gr is strongly effected by defects[16–18] and thus the sensitivity with selectivity of Gr can be tuned by functionalization or hybridization.[19,20] Gr also shows robust mechanical properties, which have attracted much attention in enduring flexible/stretchable-device integration.[21–24] Finally, a variety of approaches is possible for high-quality Gr synthesis and hybridization or modification.

Up to now, methods developed for the synthesis of Gr have been thoroughly reviewed elsewhere, including mechanical exfoliation, epitaxial growth, unzipping carbon nanotubes, etc.[25] However, only a few of these methods allowed Gr to be massively synthesized on arbitrary surfaces, especially three-dimensional (3D) architectural structures, which recently have

L. T. Duy, Dr. D.-J. Kim, Dr. T. Q. Trung, V. Q. Dang, Dr. H. K. Moon, Prof. N.-E. Lee
School of Advanced Materials Science & Engineering
Sungkynkwan University
Suwon, Kyunggi-do 440–746, Korea
B.-Y. Kim, Prof. N.-E. Lee
SKKU Advanced Institute of Nanotechnology (SAINT)
Sungkyunkwan University
Suwon, Kyunggi-do 440–746, Korea
Prof. N.-E. Lee
Samsung Advanced Institute for Health Sciences & Technology (SAIHST)
Sungkyunkwan University
Suwon, Kyunggi-do 440–746, Korea
E-mail: nelee@skku.edu

DOI: 10.1002/adfm.201401992

exhibited many interesting advantages, such as increasing surface-to-volume ratio, mass transport, reactive site density over a specific device area,[26,27] for supercapacitor [28,29] and other electrochemical applications.

For 3D gas sensors, 3D high quality Gr can be obtained chemical vapor deposition (CVD) using 3D frames of metal or composite catalysts (such as nickel foam[30], Co_3O_4 nanowire foam[31] but it is limited due to the special synthetic equipment and conditions required, such as high vacuum and temperature.[25] On the other hand, the conversion of graphene oxide (GO) to reduced graphene oxide (R-GO) via chemical or physical reducing agents (the most cost effective and easy processing method), can also yield a large continuous network of R-GO nanosheets on various sophisticated structures in various conditions.[32–34] Although this may not achieve a quality of Gr as good as CVD-grown one because R-GO nanosheets contain many defects and residual oxygen species along the basal plane and edges, these can provide the creative processability or functionality to optimize or tune the sensing performance of R-GO gas sensors.[35] Therefore, gas sensors based on R-GO and its derivatives are promising and capable of being competitive with commercial sensors.

Although extensive research activities of Gr based gas sensors on planar and hybrid structures have been undertaken over the past decade, the problems associated with the size reduction of R-GO gas sensors with enhanced performance have not been fully overcome and some challenges remain. Many researchers have focused on the development of practical low-cost gas sensors by attempting to reduce the sensor size for the enhancement of signal-to-noise ratio (SNR), resulting in the successful reduction of LOD and reduction in the additional cost with lower power consumption; however, the overall sensitivity, magnitude of transduction signal, and the interaction of the cross-section with gas molecules that mainly affects response time are diminished.[36,37] On the other hand, very few fundamental studies have been performed on utilizing the promising combination of the intrinsically enhanced surface-to-volume ratio, high responsivity of R-GO to chemical species, and high interaction cross-section of 3D micrometer scale structures for improving sensing performance. Therefore, exploiting new concepts for enhancing the performance of R-GO gas sensors by combining the structural engineering techniques of 3D microstructuring is of great interest.

In this contribution, we present an approach that can enhance the performance of R-GO chemical sensors by utilizing a simple 3D device geometry. Chemiresistor-type 3D R-GO chemical sensors were fabricated using an R-GO networked layer formed on micro-patterned pillars of SU-8 photoresist in the device channel. Comparison of gas sensing performances between two-dimensional (2D) planar and 3D micro-pillar R-GO chemical sensors was performed. Our 2D and 3D sensors were very simple, but were highly responsive to NO_2 and NH_3 gas diluted in dry synthetic air at room temperature. With high aspect-ratio 3D R-GO gas sensors (due to the extended surface-to-volume ratio as well as the increased interaction cross-section with catchment area of R-GO), the 3D sensors clearly exhibited higher sensing performance with higher transduction signal, higher sensitivity, and lower LOD than those of the 2D R-GO sensor. Our findings showed the possibility of miniaturizing the R-GO gas sensors while maintaining sufficient high sensing performance for practical low-cost gas sensors in environmental conditions. In addition, the approach here is a good premise for maximizing the advantages of the multi-scale hybridization of R-GO with a 3D structure and other dimensional materials for contemporary and future sensing devices.

2. Results and Discussion

2.1. Characterization of R-GO Gas Sensors

To study the sensing enhancement by geometrical engineering of sensing area, 2D and 3D sensor devices were designed with identical device areas with the length/width ratio of (≈400/8000 μm), as illustrated in **Figure 1**a, and fabricated in the same processes (see details in Experimental Section). The SU-8 micro-pillar array (280 × 8000 μm, 80-μm pillar diameter and 20-μm pitch) was built in the middle of the device channel area and an R-GO networked layer was formed by the reduction of GO nanosheets self-assembled on the surfaces of an atomic-layer deposited (ALD) Al_2O_3 ultra-thin layer conformally deposited on SiO_2 (2D sensor) or SU-8 micro-pillars (3D sensor). Figure 1b shows the FESEM images of as-synthesized 3D SU-8 micro-pillars with the heights of 40 μm (sample No. 3D40) and 70 μm (sample No. 3D70). The mean thickness and roughness of the R-GO layer on the Al_2O_3-coated SiO_2 surface by atomic force microscopy (AFM) were about 5 nm and 10 nm, respectively (Figure 1c). The FESEM images in Figure 1d and Figure S2 (Supporting Information) confirm that R-GO networked layer can fully cover 2D and 3D Al_2O_3 surfaces which were pretreated by PDDA. Therefore, by adjusting the pillar height (or PR thickness), we could control the total sensing area of R-GO, which was calculated and shown in **Table 1**. The surface area of the 3D40 and 3D70 samples increased by the factors of 1.97 and 2.69, respectively, compared to that of the 2D sample.

To clarify the reduction of GO nanosheets self-assembled on an Al_2O_3 layer by hydrazine vapors, we carried out Raman spectroscopy and measurements of conductance change before and after chemical reduction as shown in **Figures 2** and **3**, respectively. For Raman spectroscopy, the measurement was performed firstly to detect the existence of GO/R-GO nanosheets on the Al_2O_3-coated SiO_2 area (Figure 2a) with Al_2O_3-coated SU-8 micro-pillars (Figure 2b), and then to check the reduction by hydrazine. In Figure 2a, both the GO and R-GO samples displayed two distinctive peaks at the D band (≈1350 cm^{-1}) and G band (≈1600 cm^{-1}). The change in the intensity ratio of these peaks, I_D/I_G, was observed clearly (from 0.99 of GO to 1.03 of R-GO), which confirms that the reduction of GO had occurred.[38] In Figure 2b, both samples displayed two prominent peaks at ≈1350 cm^{-1} (D band) and ≈1600 cm^{-1} (G band), although the change of the I_D/I_G ratio was undefined. Herein, Raman spectroscopy is very sensitive to the stress/strain and roughness of a testing surface, while the SU-8 polymer surface became stressed and was rougher after CF_4/O_2 plasma treatment and conformal Al_2O_3 deposition at elevated temperature, as clearly shown in Figure S2 (Supporting Information). Additionally, structural elasticity allows GO/R-GO sheets to conform

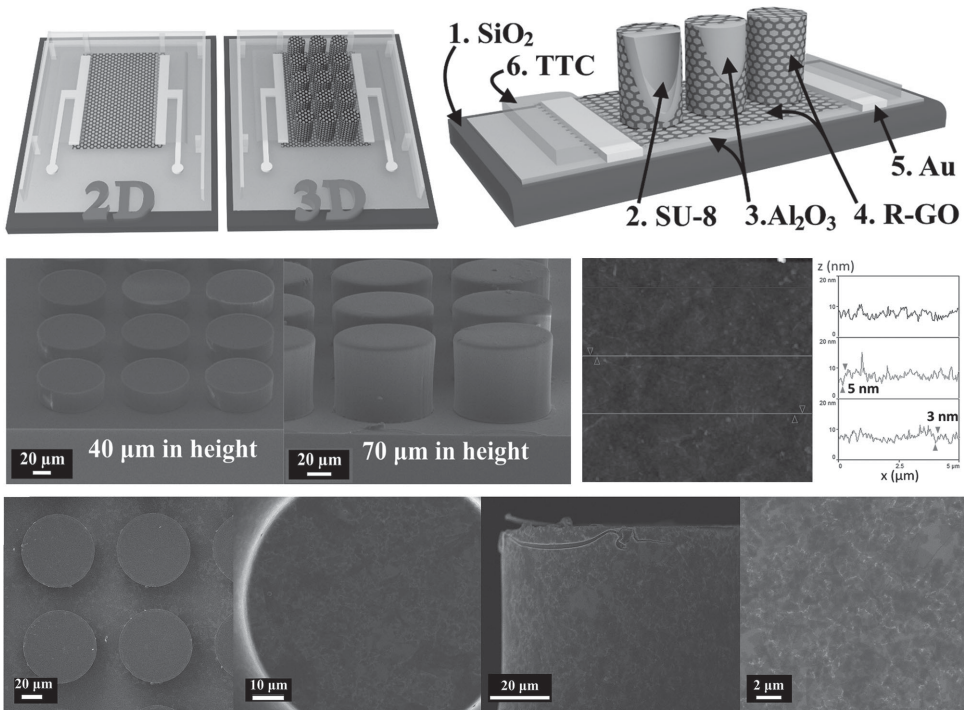

Figure 1. a) Schematic structure of both 2D and 3D devices (left) and cross-section of 3D device (right) in which the numeric digits indicate the order of fabrication steps. b) FESEM images of SU-8 pillar array with different heights of 40 (left) and 70 μm (right). c) AFM image of R-GO nanosheets assembled on PDDA-pretreated Al_2O_3 surface. d) FESEM images of R-GO networked layer covering 3D pillars on the sensing channel; low magnification top view (left), enlarged top view (second), side view (third) and enlarged side view (right), respectively.

to rough surfaces, resulting in the dominant roughness scatter in the Raman spectra.[39,40] Nevertheless, the data in Figure 2 confirm the existence of GO/R-GO on the SU-8 micro-pillars. For current-voltage (*I*–*V*) measurement, although there was no clear relationship between conductance and surface area ratio of as-fabricated 2D and 3D devices presumably due to environmental influences, a conspicuous increase in the electrical conductance before and after the reduction was observed, as shown in Figure 3a. This change verified the successful conversion of insulating GO (resistance of ~10^{11} Ω) into semi-conducting R-GO (resistance of ~10^6 Ω). In addition, Figure 3b shows the transfer curve of the R-GO devices (back-gated structure) under drain bias voltage, V_{DS} = 2 V. Due to the thick dielectric layers of SiO_2 and Al_2O_3 in the sensor, the field-effect on the channel was small. However, the plot evidently shows that the current of the transfer curve, at negative gate voltages, is much higher than that at positive gate voltages. These results indicate that after reduction, the holes are the main charge carriers of R-GO samples under an ambient condition.[40]

Table 1. Comparison of the total sensing area between 2D and 3D structures.

Sample	Channel area [μm²]	Total sensing area [cm²]	Area ratio of 3D/2D
2D	400 × 8000	0.032	–
3D40	400 × 8000	0.063	1.97
3D70	400 × 8000	0.086	2.69

2.2. Comparison of Gas Sensing Performance in 2D and 3D R-GO Structures

The response behaviors and sensitivity of the sensors were indicated as the relative change of electrical resistance, $(R - R_a)/R_a \times 100\% = \Delta R/R_a$ (%), where R_a is the initial resistance of the sensor in dry air before the exposure and R is the resistance measured during gas exposure. **Figure 4**a,b represents the comparison of intrinsic responsivity between 2D and 3D sensors towards 5-ppm NO_2 (exposure 15 min) and 40-ppm NH_3 (exposure 30 min) gases at room temperature, respectively. Because of the electron transfer between R-GO and the adsorbed gaseous molecules, the resistance to electron-withdrawing gas (NO_2) of the sensors decreased but rapidly increased to electron-donating gas (NH_3). This change concurs with the hole-doping behavior of R-GO nanosheets, as previously mentioned.

In Figure 4, the relative resistance changes of the 2D, 3D40, and 3D70 samples exposed to 5-ppm NO_2 were 19%, 21%, and 28%, respectively, while they were 20%, 75%, and 88%, respectively, when exposed to 40-ppm NH_3. This clearly indicated the trend of enhancement in responsivity to the gases by increasing the surface area and mass transport of the 3D sensors. After introducing testing gases to the chamber (Gas ON), the slope of the responsive curves of the 3D sensors and the sensor transduction signal was generally higher than that of the 2D sensors, as shown more clearly in Figure 4a. The data in Figure 4a also implies that 3D sensors detected the target molecules faster because of the increase in the catchment area as well as the interaction cross-section with gas molecules.

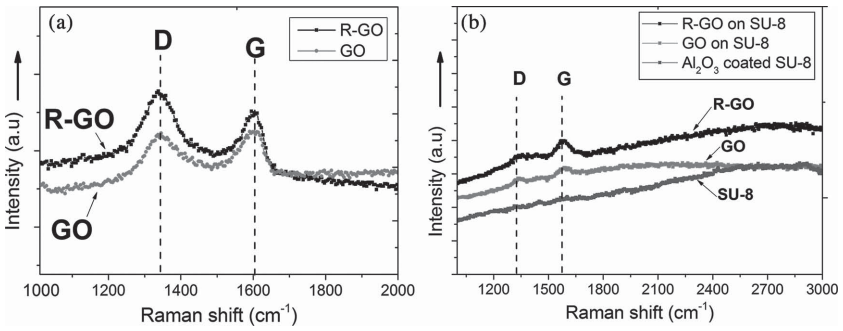

Figure 2. Raman spectra of GO/R-GO adsorbed on a) Al_2O_3-coated SiO_2 surface and b) Al_2O_3-coated SU-8 micro-pillar surface. D and G correspond to the D band (≈1350 cm^{-1}) and G band (≈1600 cm^{-1}).

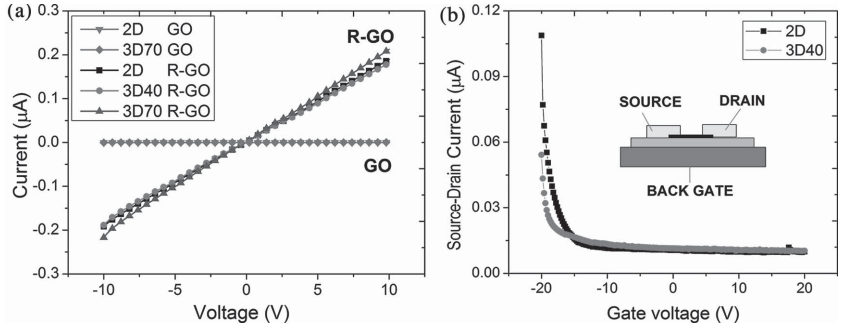

Figure 3. a) Change in the electrical conductance of the devices before and after reduction of GO networked film. b) Transfer curves of 2D and 3D40 R-GO devices under source-drain voltage (V_{DS}) of 2 V.

Analysis of the full-scale response curves shown in Figure 4b can be divided into two regions: steeply and shallow sloped regions.[41] For the steeply sloped region where the response is rapid, about 10 and 12 min was required for the 3D40 and 3D70 samples, respectively, but only ≈5 min was required for 2D samples. For the shallow sloped region where the response is slow, the 2D sensors reached saturation after gas exposure of ≈20 min; for both 3D sensors, the resistance continued gradually increasing. These results are attributed to the large interaction area of the 3D sensors. Consequently, due to the greater surface area, the 3D sensors contain more defects, edges, and other high-energy binding sites. These sites react slowly but make stronger bonds with reactive gas molecules such as NO_2 and NH_3,[18,41] resulting in the slower total recovery (gas desorption under continuous 500-sccm dry air flow at room temperature with normal lamplight condition) of the 3D sensors (≈90–100 min) compared to the 2D sensors (≈60 min). Fast recovery is still a major challenge for practical gas sensors. However, a strategy to calibrate slow-recovery R-GO sensors has been developed.[42] Besides, lengthening the rapid response region with adjusting the exposure time within this regime to reduce reactions occurring at deep energy binding sites is a good option to obtain a faster restoration, as clearly shown in Figure S3a–c (Supporting Information). After the long multi-step reduction of GO as mentioned in Experiment Section, the 3D70 sample responded rapidly, strongly, and rather stably to 40 ppm NH_3, with ≈2% change per second, but still recovered well within 15 min after multiple 2-min exposures to NO_2 and NH_3 gases. In consequence, our 3D R-GO sensor still has a potential for practical gas sensing applications at room temperature.

Herein, the mechanism of the sensing signal enhancement is mainly related to not only the increased catchment space with interaction-site density but also the amplified mass transport with interaction cross-section by vertical 3D geometry of micro-pillar arrays. However, the good self-assemblage of R-GO nanosheets to form a continuous networked layer as well as highways for charges to transport through entire 3D structures is a critical factor. Furthermore, the encapsulation layers on the two electrodes may contribute significantly to the responsive signal and recovery enhancement due to the reduction of gas diffusion in the R-GO/electrode interfaces and, in turn, their contact resistance. Therefore, with a given device area, our 3D structures allow interaction with more gas molecules within a short exposure time, leading the higher sensitivity and faster response to very small amounts of analytes at room temperature. According to Threshold Limit Values & Biological Exposure Indices, copyright 2005 by the American Conference of Governmental Industrial Hygienists (ACGIH), detection level assigned for NO_2 < 3 ppm and NH_3 < 25 ppm is important for practical sensors.[43] However, our sensors were not truthfully responsive well towards NO_2 at a concentration lower than 3 ppm, while they showed a clear responsiveness towards NH_3 gas at a wider range of concentration, as described below. At this time, the reason for low response of our R-GO material towards sub-ppm concentration of NO_2 gas is not clear, and thus we mainly focus on the NH_3 response for the comparison.

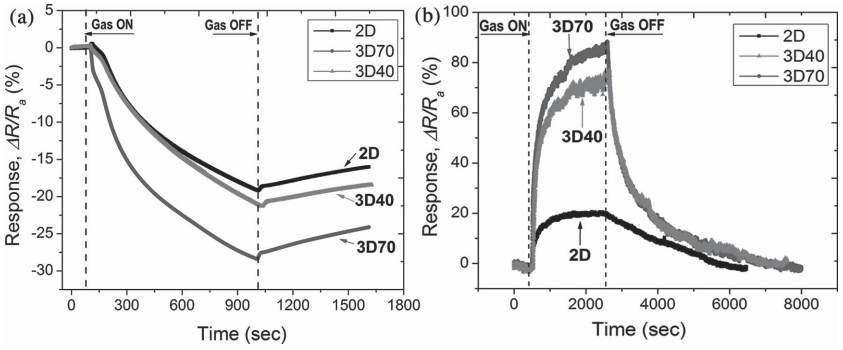

Figure 4. Sensing response of R-GO sensors towards a) 5 ppm NO_2 (exposure time ≈ 15 min) and b) 40 ppm NH_3 (exposure time ≈ 30 min).

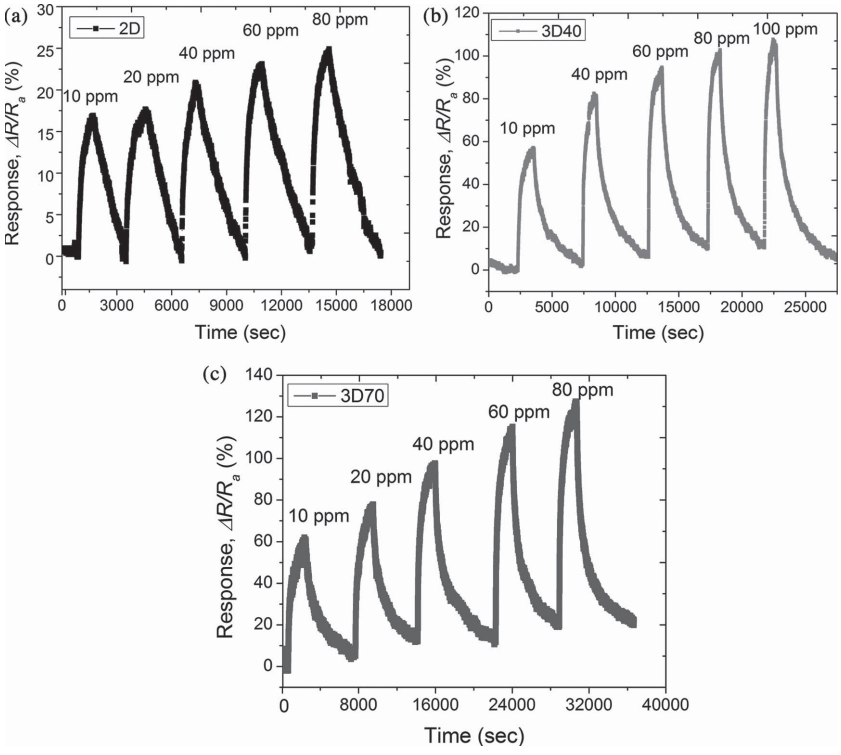

Figure 5. Responsiveness of a) 2D, b) 3D40, and c) 3D70 sensors towards various NH_3 concentrations at room temperature.

Figure 5 shows the responses of the 2D and 3D sensors to various NH_3 concentrations. Herein, the ratio of the gas exposure time (time reaching 90% maximum response, estimated from Figure 4b) to the release time (time reaching 90% of baseline, measured in Figure S4, Supporting Information)[44] was about 13/40, 21/65, and 25/80 min for the 2D, 3D40, and 3D70 samples, respectively. In Figure 5a, the relative resistance increased with increasing the NH_3 concentration in the 2D sensor. Figure 5b,c also shows the trend of the 3D sensors of the sensitivity improvement with increasing aspect ratio of micro-pillars. However, a slight baseline drift was observed in the sensors, among which the 3D70 sample showed most clearly. Therefore, to determine reliable value of sensitivity and LOD, we used a new baseline after each pulse and re-plotted as in Figure S5 (Supporting Information).

The edited plots of the response versus NH_3 concentration are illustrated in **Figure 6**. In this figure, we still see the increase in the sensor signal with increasing NH_3 concentrations. However, the plots reveal clearly that the responses of the 2D (Figure 6a) and 3D sensors (Figure 6b,c) were not linear. This was possibly due to the incomplete recovery due to partial reduction of the available interaction sites for the subsequent pulses and slow out-diffusion of gas molecules in the multilayer stacking structure of the R-GO networked layer.[45,46] The plots of the sensor signal versus NH_3 concentration showed an obvious linear regime at less than 60 ppm for both the 2D and 3D sensors.

The lowest detectable gas concentration of sensors can be extrapolated from the linear regime of the response curve versus concentration, but an analytical signal at that concentration needs to be reliably distinguished from noise signal. According to International Union of Pure and Applied Chemistry (IUPAC), LOD is obtained when the signal exceeds three times the noise level in the system.[45] The noise level and theoretical LOD of a sensor can be calculated by using the root-mean-square (RMS) deviation at the baseline and the slope of the response curve (sensitivity) as suggested by Li et al.[47] With this approach, as described in Figure S6 and Tables S1,S2 (Supporting Information), we obtained the sensitivity, RMS noise, and LOD values in the linear regime for the sensors in which the 3D sensors have a higher noise level but lower LOD (= 3×RMS/Slope) as denoted in **Table 2**. Herein, considering the 3D40 and 3D70 samples, the linear slope of the 3D70 sample is higher, with a value of about 18% ≈46% (= 0.797/0.614 ± standard error values), while its noise level is higher than that of the 3D40 sample up to 63%, resulting in the lower LOD of the 3D40 sample. Therefore, we propose that due to the compensation between sensitivity enhancement and noise level, 3D sensors exhibit lower LOD than 2D sensors. Utilizing 3D sensor geometry is shown to clearly improve the sensing performance at a given device size. Compared to other room-temperature ammonia gas sensors based on R-GO and Gr based materials (see **Table 3**), the obtained detection range of our 3D devices is comparable. Optimization of sensor design and fabrication process is necessary to further lower the LOD of 3D gas sensor.

3. Conclusion

In summary, our R-GO based sensors were fabricated in 2D and 3D structures, and both sensors exhibited a high sensitivity towards NH_3 at room temperature. According to the initial purpose, we completed the fundamental comparison of performances between our 2D and 3D R-GO sensors. With the supporting of SU-8 micro-pillar array, the magnitude of transduction signal as well as the overall sensing performance of the 3D devices improved significantly compared to those of the 2D devices. Although possessing a large surface area and thus higher noise level, 3D sensors still revealed a lower LOD. The above results indicated the capability of this 3D micro-pillar structure for useful R-GO sensors to detect NH_3 at room temperature. At the moment, a clear rational relationship between the total sensing area with enhancement of transduction signal, sensitivity, and LOD was not able to be clearly determined. However, this preliminary study on 3D R-GO chemical sensors provides us with the opportunity to not only miniaturize the sensor for lowering LOD but also still obtain a sufficiently high sensing performance for the large-scale integration. Furthermore, the outstanding surface properties of nano-scale materials (0D, 1D,

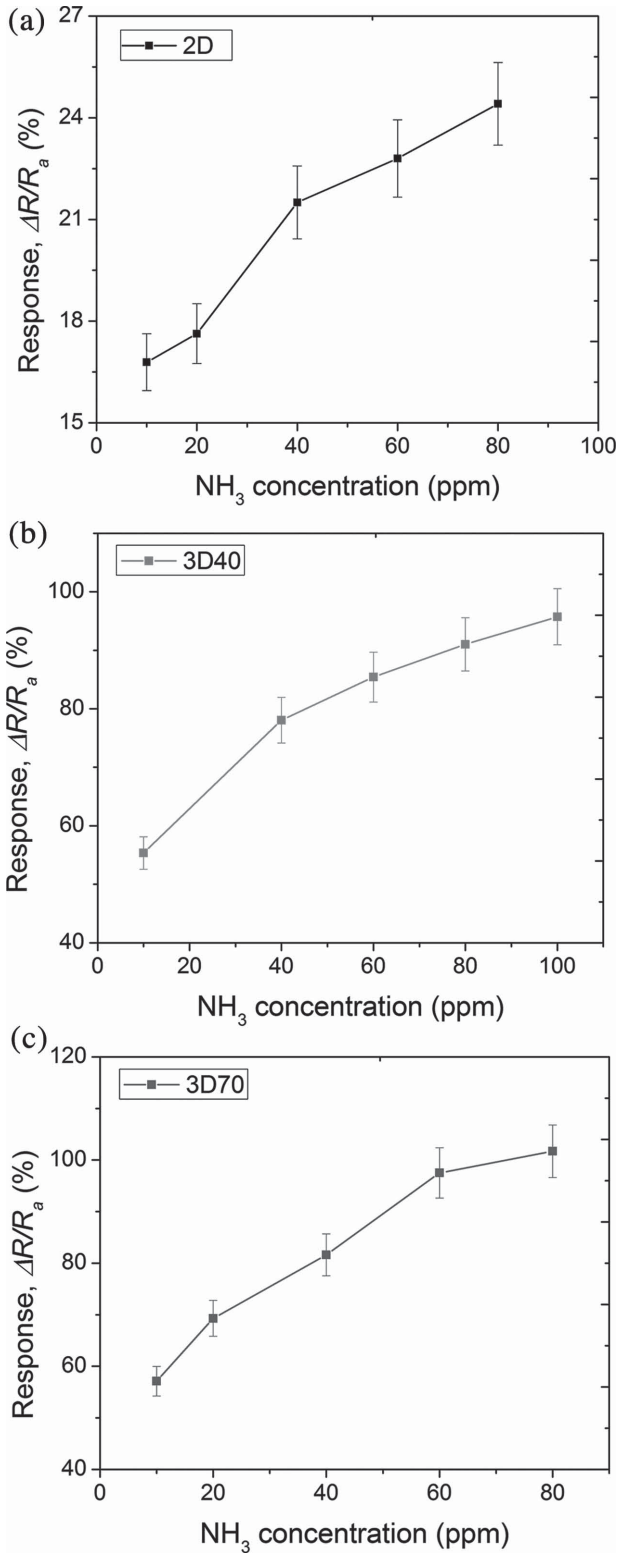

Figure 6. Response curves versus NH_3 concentration for a) 2D, b) 3D40 and c) 3D70 R-GO sensors after a new base line was used.

or 2D) hybridized with 3D micro-scale structures might allow us to exploit further improvements of the various chemical sensing devices.

Table 2. Comparison of the noise level and LOD between 2D and 3D sensors.

Sample	Surface ratio [3D/2D]	Sensitivity [ppm^{-1}]	Standard Error [ppm^{-1}]	RMS Noise [%]	LOD [ppm]
2D	–	0.128	0.007	0.086	2.025 ± 0.111
3D40	1.97	0.614	0.107	0.244	1.193 ± 0.208
3D70	2.69	0.797	0.055	0.399	1.501 ± 0.104

4. Experimental Section

Preparation of 3D SU-8 Micro-Pillar Array: After cleaning with Piranha, acetone, ethanol, and deionized (DI) water with sonication and heated at 200 °C for vapor desorption, silicon dioxide (SiO_2)/Si wafers were primed with hexamethyldisilazane (Acros Organics) to form a hydrophobic surface to enhance the adhesion of SU-8. SU-8 2050 PR (MicroChem) was spin coated on the wafer to build micro-pillar arrays with 40 μm (spinning speed of 4000 rpm) and 70 μm (spinning speed of 2000 rpm) thicknesses. Exposure doses for 40- and 70-μm patterns were 250 and 350 mJ/cm^2, respectively. After development of PR with the SU-8 developer (MicroChem) and then isopropanol (IPA), the clear patterns were followed by a 3-min treatment with CF_4/O_2 plasma by chemical dry etching (CDE) system to remove the residual PR. The samples were then cured at 200 °C for 30 min on a hotplate.

Fabrication of 2D and 3D R-GO Sensors: The fabrication of 2D and 3D sensors was carried out using the same processes. For the 2D devices, we also used PR patterning to define the channel and device areas. For 3D devices, the SU-8 micro-pillars formed on a SiO_2/Si wafer were used. GO platelets (Graphene Market) were suspended in DI water (1 mg/mL). The stable of aqueous dispersion was obtained by magnetically stirring at 1000 rpm for 2 h, following 12-h sonication at room temperature, and finally centrifuging at 3000 rpm for 30 min to remove the large residuals. Due to the different surface properties of SiO_2 and SU-8, the adsorption of GO on the planar SiO_2 surface (SiO_2/Si wafer) would differ from that on the surface of the SU-8 micro-pillars. Thus, to form a thin continuous GO network for comparison of the 2D and 3D sensors, a conformal 50-nm-thick- aluminum oxide (Al_2O_3) layer was deposited for all 2D and 3D samples at 200 °C by atomic layer deposition (ALD). Poly(diallyldimethylammonium chloride (PDDA) 20 wt% in water, Sigma Aldrich) was then used to modify the Al_2O_3 surface to enhance the adsorption of GO nanosheets. Because the rapid response region increases with increasing reduction time of GO,[50] our GO was reduced by 2 steps using hydrazine vapor (hydrazine monohydrate 99+%, Alfa Aesar) at 60 °C for 20 h and then annealed at 200 °C for 2 h in dry N_2 flow at atmospheric pressure. Cr (10 nm) and Au (50 nm) electrodes were then deposited through shadow-masks by electron beam and thermal evaporation, respectively. Finally, to minimize the change of contact resistance due to the diffusion of gas molecules in the metal electrode/R-GO interface during measurement (which contributes to the overall sensing response of the sensors),[51] the 100-nm Tetratetracontane (TTC) layer as an encapsulation layer was deposited at high vacuum (10^{-6} Torr) using a thermal evaporation system.

Characterization: FE-SEM and AFM measurements were carried out with JEOL JSM-6500F and INNOVA, respectively. Raman spectra were recorded by using Alpha300 R (WITec) with 532-nm laser excitation. *I–V* characteristics were measured with an HP 4145B semiconductor parameter analyzer.

Gas Sensing Measurement: The sensing measurements were performed in a gas sensing system with gas supply and control units as shown in Figure S1 in the Supporting Information. To reduce the electrical contact noise, we used open-cavity ceramic packaging (Spectrum) and gold wire bonding. The device was loaded into a testing glass tube chamber placed in a thermostatic furnace. The temperature inside the chamber was stabilized at 300 ± 1 K. Dry synthetic air

Table 3. Comparison of detectable levels of some ammonia sensors based on R-GO and Gr materials.

Resistor devices	Sensing enhancement method			Detectable level [ppm]	Ref.
	Interdigitated electrodes	Modified materials	Increased surface area		
R-GO on 3D pillars	–	–	Yes	≈1–100	Current work
R-GO on MEMS platform	Yes	–	–	≈5	[11]
R-GO/polypyrrole nanofibers	Yes	Yes	–	0.001–50	[13]
R-GO/copper phthalocyanine	Yes	Yes	–	0.4–3200	[48]
Gr/polyaniline composite	Yes	Yes	–	1–6400	[49]
CVD Gr foam	–	–	Yes	20–1000	[30]

(21% v/v O_2/N_2), that is, carrier gas, was used for purging and dilution. The maximum flow rate (500 sccm) of the carrier gas was maintained as constant. The maximum concentration of 500-sccm testing gas was 5 ppm for NO_2 in air and 100 ppm for NH_3 in air. Further dilution was controlled manually through mass flow controllers (MFC). Electrical currents were monitored using a Keithley 2400 meter. The implemented software (Keithley) allowed control of the bias voltage (2 V), limit current (10 mA), and recording output signal of the current and resistance.

Supporting Information

Supporting Information is available from the Wiley Online Library or from the author, including: diagram of the sensing measurement system; FESEM images of 3D surfaces after Al_2O_3 deposition; high sensing performance of 3D70 R-GO sensors; measurement of recovery time for R-GO sensors; and calculation of noise level and detection limit.

Acknowledgements

This research was supported by the Basic Science Research Program (Grant No. 2010–0015035 and 2013R1A2A1A01015232) and the Fundamental Technology R&D Program for Society (Grant number : 2013M3C8A3075845) through the National Research Foundation (NRF) funded by the Ministry of Science, ICT& Future Planning.

Received: June 17, 2014
Revised: October 16, 2014
Published online: December 5, 2014

[1] W. Yuan, G. Shi, *J. Mater. Chem. A* **2013**, *1*, 10078.
[2] G. Jimenez-Cadena, J. Riu, F. X. Rius, *Analyst* **2007**, *132*, 1083.
[3] A. Tricoli, M. Righettoni, A. Teleki, *Angew. Chem. Int. Ed.* **2010**, *49*, 7632.
[4] L. Jia, W. Cai, *Adv. Funct. Mater.* **2010**, *20*, 3765.
[5] G. Konvalina, H. Haick, *Acc. Chem. Res.* **2013**, *47*, 66.
[6] R. A. Potyrailo, C. Surman, N. Nagraj, A. Burns, *Chem. Rev.* **2011**, *111*, 7315.
[7] W. J. Park, M. H. Kim, B. H. Koo, W. J. Choi, J.-L. Lee, J. M. Baik, *Sens. Actuators B Chem.* **2013**, *185*, 10.
[8] E. Llobet, *Sens. Actuators B Chem.* **2013**, *179*, 32.
[9] J. Gutiérrez, M. C. Horrillo, *Talanta* **2014**, *124*, 95.
[10] F. Schedin, A. K. Geim, S. V. Morozov, E. W. Hill, P. Blake, M. I. Katsnelson, K. S. Novoselov, *Nat. Mater.* **2007**, *6*, 652.
[11] J. D. Fowler, M. J. Allen, V. C. Tung, Y. Yang, R. B. Kaner, B. H. Weiller, *ACS Nano* **2009**, *3*, 301.
[12] R. K. Paul, S. Badhulika, N. M. Saucedo, A. Mulchandani, *Anal. Chem.* **2012**, *84*, 8171.
[13] N. Hu, Z. Yang, Y. Wang, L. Zhang, Y. Wang, X. Huang, H. Wei, L. Wei, Y. Zhang, *Nanotechnology* **2014**, *25*, 025502.
[14] A. Lipatov, A. Varezhnikov, P. Wilson, V. Sysoev, A. Kolmakov, A. Sinitskii, *Nanoscale* **2013**, *5*, 5426.
[15] S. Rumyantsev, G. Liu, M. S. Shur, R. A. Potyrailo, A. A. Balandin, *Nano Lett.* **2012**, *12*, 2294.
[16] A. Salehi-Khojin, D. Estrada, K. Y. Lin, M.-H. Bae, F. Xiong, E. Pop, R. I. Masel, *Adv. Mater.* **2012**, *24*, 53.
[17] B. Kumar, K. Min, M. Bashirzadeh, A. B. Farimani, M.-H. Bae, D. Estrada, Y. D. Kim, P. Yasaei, Y. D. Park, E. Pop, N. R. Aluru, A. Salehi-Khojin, *Nano Lett.* **2013**, *13*, 1962.
[18] L. K. Randeniya, H. Shi, A. S. Barnard, J. Fang, P. J. Martin, K.(Ken) Ostrikov, *Small* **2013**, *9*, 3993.
[19] W. Yuan, A. Liu, L. Huang, C. Li, G. Shi, *Adv. Mater.* **2013**, *25*, 766.
[20] W. Li, X. Geng, Y. Guo, J. Rong, Y. Gong, L. Wu, X. Zhang, P. Li, J. Xu, G. Cheng, M. Sun, L. Liu, *ACS Nano* **2011**, *5*, 6955.
[21] C. Yan, J. H. Cho, J.-H. Ahn, *Nanoscale* **2012**, *4*, 4870.
[22] S. H. Chae, Y. H. Lee, *Nano Converg.* **2014**, *1*, 1.
[23] S. J. Park, O. S. Kwon, S. H. Lee, H. S. Song, T. H. Park, J. Jang, *Nano Lett.* **2012**, *12*, 5082.
[24] M. Kim, C. Lee, J. Jang, *Adv. Funct. Mater.* **2014**, *24*, 2489.
[25] M. Liu, R. Zhang, W. Chen, *Chem. Rev.* **2014**, *114*, 5117.
[26] Y. J. Yun, W. G. Hong, N.-J. Choi, H. J. Park, S. E. Moon, B. H. Kim, K.-B. Song, Y. Jun, H.-K. Lee, *Nanoscale* **2014**, *6*, 6511.
[27] M. Melli, G. Scoles, M. Lazzarino, *ACS Nano* **2011**, *5*, 7928.
[28] U. N. Maiti, J. Lim, K. E. Lee, W. J. Lee, S. O. Kim, *Adv. Mater.* **2014**, *26*, 615.
[29] J. Zhi, W. Zhao, X. Liu, A. Chen, Z. Liu, F. Huang, *Adv. Funct. Mater.* **2014**, *24*, 2013.
[30] F. Yavari, Z. Chen, A. V. Thomas, W. Ren, H.-M. Cheng, N. Koratkar, *Sci. Rep.* **2011**, *1*.
[31] X.-C. Dong, H. Xu, X.-W. Wang, Y.-X. Huang, M. B. Chan-Park, H. Zhang, L.-H. Wang, W. Huang, P. Chen, *ACS Nano* **2012**, *6*, 3206.
[32] S. Basu, P. Bhattacharyya, *Sens. Actuators B Chem.* **2012**, *173*, 1.
[33] C. K. Chua, M. Pumera, *Chem. Soc. Rev.* **2013**, *43*, 291.
[34] Y. Guo, B. Wu, H. Liu, Y. Ma, Y. Yang, J. Zheng, G. Yu, Y. Liu, *Adv. Mater.* **2011**, *23*, 4626.
[35] J. K. Wassei, R. B. Kaner, *Acc. Chem. Res.* **2013**, *46*, 2244.
[36] N. K. Rajan, D. A. Routenberg, M. A. Reed, *Appl. Phys. Lett.* **2011**, *98*, 264107.
[37] P. E. Sheehan, L. J. Whitman, *Nano Lett.* **2005**, *5*, 803.
[38] D. R. Dreyer, S. Park, C. W. Bielawski, R. S. Ruoff, *Chem. Soc. Rev.* **2010**, *39*, 228.
[39] W. Zhang, X. Cui, B.-S. Yeo, T. Schmid, C. Hafner, R. Zenobi, *Nano Lett.* **2007**, *7*, 1401.
[40] M. P. Pujadó, In *Carbon Nanotubes as Platforms for Biosensors with Electrochemical and Electronic Transduction*; Springer Theses; Springer Berlin Heidelberg **2012**, pp 1–78.

[41] J. T. Robinson, F. K. Perkins, E. S. Snow, Z. Wei, P. E. Sheehan, *Nano Lett.* **2008**, *8*, 3137.
[42] G. Lu, S. Park, K. Yu, R. S. Ruoff, L. E. Ocola, D. Rosenmann, J. Chen, *ACS Nano* **2011**, *5*, 1154.
[43] ACGIH, In *2005 TLVs and BEIs Based on the Document of the Threshold Limit Values for Chemical Substances and Physical Agents & Biological Exposure Indices*; American Conference of Governmental Industrial Hygienists (ACGIH): Cincinnati, Ohio, 2005; p. 8–29.
[44] M. M. Arafat, B. Dinan, S. A. Akbar, A. S. M. A. Haseeb, *Sensors* **2012**, *12*, 7207.
[45] J. Hassinen, J. Kauppila, J. Leiro, A. Määttänen, P. Ihalainen, J. Peltonen, J. Lukkari, *Anal. Bioanal. Chem.* **2013**, *405*, 3611.
[46] H. Y. Jeong, D.-S. Lee, H. K. Choi, D. H. Lee, J.-E. Kim, J. Y. Lee, W. J. Lee, S. O. Kim, S.-Y. Choi, *Appl. Phys. Lett.* **2010**, *96*, 213105.
[47] J. Li, Y. Lu, Q. Ye, M. Cinke, J. Han, M. Meyyappan, *Nano Lett.* **2003**, *3*, 929.
[48] X. Zhou, X. Wang, B. Wang, Z. Chen, C. He, Y. Wu, *Sens. Actuators B Chem.* **2014**, *193*, 340.
[49] Z. Wu, X. Chen, S. Zhu, Z. Zhou, Y. Yao, W. Quan, B. Liu, *Sens. Actuators B Chem.* **2013**, *178*, 485.
[50] F. Yavari, N. Koratkar, *J. Phys. Chem. Lett.* **2012**, *3*, 1746.
[51] G. Lu, L. E. Ocola, J. Chen, *Nanotechnology* **2009**, *20*, 445502.